

Germacrone induces caspase-3/GSDME activation and enhances ROS production, causing HepG2 pyroptosis

XINFENG SUN^{1,2*}, XIN ZHONG^{1,2*}, WENFENG MA^{1,2*}, WENXING FENG^{1,2}, QI HUANG^{1,2}, MENGQING MA^{1,2}, MINLING LV^{1,2}, RUI HU^{1,2}, ZHIYI HAN^{1,2}, JING LI^{1,2} and XIAOZHOU ZHOU^{1,2}

¹Department of Liver Disease, Shenzhen Traditional Chinese Medicine Hospital; ²Department of Liver Disease, The Fourth Clinical Medical College of Guangzhou University of Chinese Medicine, Shenzhen, Guangdong 518033, P.R. China

Received March 2, 2022; Accepted April 14, 2022

DOI: 10.3892/etm.2022.11383

Abstract. Liver cancer is a highly lethal malignancy. Despite considerable efforts made in recent years, the prognosis of patients with liver cancer remains poor. *Curcuma zedoaria* (known as Ezhu in Chinese) is widely prescribed in traditional Chinese medicine. Germacrone (GM) is a sesquiterpene constituent derived from the essential oil of Ezhu, and exerts anti-carcinogenic effects by inducing apoptosis in various cancer cells. The present study investigated the potential mechanism of GM in HepG2 cells. Cell Counting Kit-8, colony-formation and lactate dehydrogenase-release assays, as well as cell death assays using flow cytometry, were performed to evaluate HepG2 cell proliferation following GM treatment. HepG2 cells were transfected with caspase-3 small interfering RNA and then treated with GM. Caspase-3 expression levels were determined by reverse transcription-quantitative PCR and western blotting. The present study showed that GM inhibited the growth of HepG2 cells and induced the proteolytic cleavage of caspase 3, with concomitant cleavage of gasdermin E (GSDME), by markedly increasing the production of reactive oxygen species (ROS). This led to caspase 3-dependent cleavage of GSDME, thereby promoting pyroptosis in HepG2 cells. However, these changes were rescued by ROS scavengers,

such as N-acetylcysteine. Furthermore, GM inhibited tumor growth by promoting the cleavage of caspase 3 and GSDME in HepG2 cell xenograft models. These results indicated that GM induced GSDME-dependent pyroptosis through caspase 3 activation, at least in part, by damaging the mitochondria and enhancing ROS production, thereby supporting the possible development of GM as a candidate for the prevention and treatment of liver cancer.

Introduction

Liver cancer is the fourth leading cause of cancer-related death worldwide. The main risk factors for its development are liver cirrhosis, chronic hepatitis B or C virus infection, and alcoholic and non-alcoholic fatty liver diseases (1-3). According to the latest global cancer burden statistics released by the International Agency for Research on Cancer of the World Health Organization, China reported the highest incidence of liver cancer cases in 2020, with ~4,568,754 new cases that year. Moreover, liver cancer is the second leading cause of all cancer deaths in China, posing a serious threat to overall health and quality of life (4). Exhaustive research on liver cancer has yielded a considerable improvement in the monitoring methods and treatment strategies available for this disease (1). However, most patients with liver cancer are diagnosed in the middle and advanced stages of the disease, and therefore cannot undergo surgical resection. Additionally, most available drugs for liver cancer are non-specific, which causes liver cancer cells to easily develop resistance to single-target drugs (2). Consequently, the mortality rate of liver cancer remains high, with a 5-year survival rate of <5% (3). Therefore, there is an urgent need to develop new and effective drugs to improve the overall survival of patients with liver cancer and their quality of life.

Traditional Chinese medicine is widely used for cancer treatment in China, as the numerous natural compounds employed target various cellular processes and cause relatively few adverse reactions (5,6). Additionally, certain compounds have demonstrated high efficiency and reduced toxicity as curative agents for liver cancer (7). *Curcuma zedoaria* (referred to as Ezhu in traditional Chinese medicine) is a herb commonly used for alleviating blood stasis and stagnation (8) or for treating heart and abdominal pain, swelling or food stagnation (9,10);

Correspondence to: Professor Xiaozhou Zhou, Department of Liver Disease, Shenzhen Traditional Chinese Medicine Hospital, 1 Fuhua Road, Futian, Shenzhen, Guangdong 518033, P.R. China
E-mail: zxz1006@gzucm.edu.cn

*Contributed equally

Abbreviations: CCK-8, Cell Counting Kit-8; CYP, cytochrome P450; DHE, dihydroethidium; DMEM, Dulbecco's modified Eagle's medium; ECL, enhanced chemiluminescence; FBS, fetal bovine serum; GSDMD, gasdermin D; GSDME, gasdermin E; GM, germacrone; LDH, lactate dehydrogenase; NAC, N-acetylcysteine; PI, propidium iodide; ROS, reactive oxygen species; TEM, transmission electron microscopy

Key words: *curcuma zedoaria*, liver cancer, anti-carcinogenic effects, gasdermin E

it is also widely prescribed in traditional Chinese medicine for anti-tumor therapy and displays anti-carcinogenic properties believed to promote the flow of Qi, a concept in traditional Chinese medicine that represents the vital life force dredging the meridians, reducing lumps and relieving pain (11,12). Several studies have confirmed that *Curcuma zedoaria* yields a beneficial effect in the treatment of various tumors; it also exerts a substantial inhibitory effect on the proliferation of cervical and breast cancer, and other tumors (13-15). The chemical composition of *Curcuma zedoaria* is complex and may be roughly categorized into volatile oils and curcumin (9). Germacrone (GM) is a volatile oil present in all varieties of *Curcuma zedoaria* at relatively stable concentrations. GM has been demonstrated to possess a wide range of pharmacological properties, thereby rendering it an efficacious therapeutic candidate against several types of cancer (16,17). Although several studies have reported that GM inhibits HepG2 cell growth (18,19), the mechanism underlying this inhibition remains unclear.

Pyroptosis is a newly discovered mechanism of pro-inflammatory programmed cell death distinct from apoptosis, necrosis and autophagy (20-22). The main manifestation is cell swelling and lysis, accompanied by the release of pro-inflammatory factors (22). Classic pyroptosis is mediated by caspases-1/4/5/11, which cleave the effector gasdermin D (GSDMD), canceling the auto-inhibition that the C-terminal domain of GSDMD exerts over the pro-active N-terminal GSDMD domain (23-25). Thereafter, the activated N-terminal GSDMD fragment oligomerizes and perforates the cellular membrane, causing pyroptosis (25,26). Wang *et al.* (26) found that there is a very conservative caspase-3 tetrapeptide cleavage site in the GSDME. In specific cells expressing GSDME, activation of caspase-3, under certain conditions, can specifically cleave GSDME and release the N-terminus, thus forming membrane pores in the plasma membrane and triggering the lytic death of the cells. Therefore, GSDME may act as an effector of secondary necrosis in response to certain physiological stimuli. This strategy may provide an effective host response when in contact with certain pathogens that block the apoptotic pathway (26,27). Curcumin has been reported to promote the lysis of GSDME protein in HepG2 cells, while also inducing pyrolysis and exerting anticancer effects (28). Additionally, Zhang *et al.* (29) found that miltirone induces HepG2 cell death through GSDME-dependent pyroptosis, which indicates that HepG2 cells have high levels of GSDME protein expression. Another study demonstrated that the concentration of GM induces a dose-dependent increase in activated caspase-3 expression in HepG2 cells (18). Despite these indications, it remains unclear whether GM activates caspase-3, inducing the cleavage of GSDME and cell pyroptosis, and whether it exerts anticancer effects.

The present study investigated the effects of GM on HepG2 cells using *in vitro* and *in vivo* models, and elucidated the possible molecular mechanisms, with a special focus on the ability of GM to induce pyroptosis in HepG2 cells.

Materials and methods

Reagents. Antibodies against caspase-3 (cat. no. ab184787), GSDMD-N (cat. no. ab215203), GSDMD (cat. no. ab210070),

pro-caspase-1 + p10 + p12 (cat. no. ab179515) and GSDME/GSDME-N-terminal (cat. no. ab215191) were purchased from Abcam. Antibodies against cleaved caspase-3 (cat. no. 19677-1-AP) and GAPDH (cat. no. 60004-1-1g), and horseradish peroxidase-conjugated secondary antibodies (cat. no. SA00001-1) were purchased from ProteinTech Group, Inc. The Cell Counting Kit-8 (CCK-8) (cat. no. C0037), BeyoClick™, EdU Cell Proliferation Kit with Alexa Fluor 488 (cat. no. C0071S), propidium iodide (PI; cat. no. ST511), 7-AAD Cell Viability Assay Kit (cat. no. C1053S) were purchased from Beyotime Institute of Biotechnology. GM (cat. no. S9311; purity: 98.2%) and N-acetylcysteine (NAC; cat. no. S1623) were purchased from Selleck Chemicals.

Cell culture and treatment. HepG2 cells were purchased from the Cell Bank of the Chinese Academy of Sciences and authenticated by STR profiling. HepG2 cells were primarily cultured in Dulbecco's modified Eagle's medium (DMEM; Hyclone; Cytiva) supplemented with 10% fetal bovine serum (FBS) and 1% penicillin-streptomycin in an incubator at 37°C, under 5% CO₂ (18). Cells were treated with 0, 50, 100, 150 and 200 μM GM at 37°C for 12, 24 or 48 h, following which different assays were performed. HepG2 cells were pretreated with or without 5 mM NAC for 2 h before treatment with 200 μM of GM for 24 h, following which different assays were performed.

PI staining. HepG2 cells were pretreated with 0, 50, 100, 150 and 200 μM GM at 37°C for 24 h, a PI solution (Beyotime Institute of Biotechnology) was added to the medium and further incubated for 30 min at 37°C in the dark. Observed under a fluorescence microscope (Leica Microsystems, Inc.), in three random sections of each sample, three different areas (or more) were randomly selected for the capture of images. Analyses were performed using ImageJ 1.8.0 software (National Institutes of Health). Results are shown as the mean ± SD.

Cell viability assay. Cell viability was evaluated using CCK-8 and colony formation assays. For the colony formation assay, the cells were plated at a density of 500 cells/well in a 6-well plate (Corning, Inc.) and then cultured for 7 days in the aforementioned culture medium. The following day, the cells were treated with the desired doses (0, 50, 100, 150 and 200 μM) of GM for 24 h, and then the culture medium was refreshed. The culture was continued for 7 days and the medium was changed every 3 days. The cells were then washed twice with PBS, fixed in methanol for 10 min at 37°C and stained with 1% crystal violet for 10 min at 37°C and manually counted. Cell groups consisting of >50 cells were considered colonies. For the CCK-8 assay, a total of 10,000 cells per well were seeded into 96-well plates, incubated for 12 h and subsequently exposed to the desired doses of GM (0, 50, 100, 150, and 200 μM) for 12, 24 or 48 h. Cell viability was measured with a Cell Counting Kit-8 after GM treatment at a wavelength of 450 nm. Cell proliferation was measured with a BeyoClick™ EdU Cell Proliferation Kit with Alexa Fluor 488 after GM (0, 50, 100, 150 and 200 μM) treatment for 24 h. For microscopic analysis, images of the same area were obtained from three different experiments. Analyses were performed using ImageJ 1.8.0

software (National Institutes of Health). Results are expressed as the mean \pm SD.

Flow cytometry. Flow cytometry was performed using an Annexin V-FITC/PI apoptosis detection kit (Nanjing KeyGen Biotech Co., Ltd.), according to the manufacturer's instructions. Briefly, HepG2 cells treated with/without GM for 24 h were digested with trypsin in the absence of EDTA. After digestion, the harvested cells were washed with PBS and resuspended in 500 μ l binding buffer. Cells were then incubated with a binding buffer containing 5 μ l Annexin V-FITC and 5 μ l PI for 15 min at 25°C in the dark. The cells were analyzed using CytExpert 2.0 software (Beckman Coulter, Inc.).

LDH release assay. HepG2 cells in the logarithmic growth phase were seeded in a 96-well plate at a density of 5×10^3 cells per well. Cells were incubated overnight in a cell incubator at 37°C under 5% CO₂, and subsequently exposed to different GM concentrations (0, 50, 100, 150 and 200 μ M) for 12, 24 or 48 h. The LDH release assay was performed according to instructions in the LDH Cytotoxicity Assay Kit (Beyotime Institute of Biotechnology).

Cell death assay. For the cell death assay, HepG2 cells were pretreated with GM at different concentrations (0, 50, 100, 150 and 200 μ M) for 24 h. Cells were collected and initially stained with 7-AAD (2 μ g/ml in PBS; Nanjing KeyGen Biotech Co., Ltd.) for 30 min, and washed three times with PBS (for 3 min each), and resuspended in 500 μ l 1X Assays Buffer. The cells were then analyzed using CytExpert 2.0 software (Beckman Coulter, Inc.), and data were collected for analysis.

Western blotting. Cells or tumor tissues were washed with cold PBS twice and prepared in radioimmunoprecipitation assay (RIPA) lysis buffer (Beyotime Institute of Biotechnology) containing protease/phosphatase inhibitor cocktail. The BCA Protein Assay Kit (Beyotime Institute of Biotechnology) was used to measure the protein concentration. Total proteins (30 μ g) were separated on 12% gels using SDS-PAGE and then transferred onto nitrocellulose membranes. Next, the membranes were blocked in Tris-buffered saline containing 0.1% Tween-20 and 5% fat-free milk for 1 h at 25°C, followed by incubation with primary antibody solutions (1:1,000) for 18 h at 4°C. Subsequently, the membranes were incubated with secondary antibody solutions (1:5,000) at 25°C for 1 h. Enhanced chemiluminescence (ECL) reagent (MilliporeSigma) or ECL Plus Amersham; Cytiva) were used to detect the immunoreactive bands and visualized with the ChemiDoc XRS system (Bio-Rad Laboratories, Inc.). Densitometry analysis for western blotting was performed using Gelpro32 imaging software (Media Cybernetics, Inc.).

Reverse transcription-quantitative PCR (RT-qPCR). Total RNA was isolated from the cells or tissues using an RNAprep FastPure kit (cat. no. TSP413; TsingKe Biological Technology), according to the manufacturer's instructions. Total RNA was reverse transcribed into complementary DNA using an RT6 cDNA Synthesis Kit (cat. no. TSK302M; TsingKe Biological Technology), according to the manufacturer's instructions. qPCR was performed using a CFX96 Real-time

System (Bio-Rad Laboratories, Inc.) with SYBR Green I (cat. no. TSE202; TsingKe Biological Technology) and thermocycling conditions as follows: 95°C for 10 sec, 61°C for 30 sec and 72°C for 30 sec, for 40 cycles. Relative gene expression levels were calculated using the 2^{- $\Delta\Delta$ C_q} method (30). The primer sense and antisense sequences were as follows: β -actin forward, 5'-CCTGGCACCCAGCACAAT-3' and reverse, 5'-GGGCCG GACTCGTCATAC-3'; and caspase-3 forward, 5'-TGGAAC AAATGGACCTGTTGACC-3' and reverse, 5'-AGGACTCAA ATTCTGTTGCCACC-3'. β -actin was used as an internal control for quantification.

Transmission electron microscopy (TEM). HepG2 cells were pretreated with GM at different concentrations (0, 50, 100, 150 and 200 μ M) for 24 h. The cells were fixed with 4% paraformaldehyde at 4°C for 48 h, post-fixed in 1% osmium tetroxide at 4°C for 1.5 h, dehydrated in a graded ethanol series, infiltrated with propylene oxide, embedded in epoxy resins at 37°C for 12 h and sectioned to a thickness of 70 nm. After double staining with uranyl acetate (25°C for 30 min) and lead citrate (25°C for 5 min), ultrathin sections were examined using a model HT-7700 transmission electron microscope (Hitachi Ltd.).

Cell transfection. HepG2 cells were transfected with caspase-3 small interfering (si)RNA (5'-GCAGCAAACCTCAGGGAA ATT-3') and control siRNA (5'-TTCTCCGAACGUGUC ACGUTT-3'), purchased from Guangzhou RiboBio Co., Ltd., following the manufacturer's instructions. siRNA (100 nM) transfections were performed using Lipofectamine[®] 2000 transfection reagent (Gibco; Thermo Fisher Scientific, Inc.) according to the manufacturer's instructions at 37°C for 48 h. Opti-MEM (Gibco; Thermo Fisher Scientific, Inc.) transfection medium was replaced with complete culture medium with 10% fetal bovine serum 5 h after transfection. All experiments were performed 48 h after the transfection. The expression of caspase-3 was measured by RT-qPCR and western blotting.

Nude mouse xenograft model. Female nude mice (BALB/c; age, 4 weeks; weight, 20-22 g), were purchased from the Laboratory Animal Center of Guangzhou University of Chinese Medicine (Shenzhen, China). All mice were housed under the following conditions: A 12 h light/dark cycle (lights on, 07:00; lights off, 19:00), a temperature of 22 \pm 2°C, a humidity of 50 \pm 10%, and free access to standard diet and water. All animal experiments were approved by the Animal Ethics Committee of Guangzhou University of Chinese Medicine (approval no. 20210303042). As described in a previous study (29), mice (n=30) were randomly assigned to five treatment groups (n=6), and then treated with GM solution (5, 10, 15 or 20 mg/kg body weight) or the same dose of vehicle (PBS). Briefly, 1 \times 10⁶ HepG2 cells were resuspended in 100 μ l PBS and injected subcutaneously into the right side of the mouse. Starting 6 days after cell injection, the nude mice were treated intragastrically with GM solution (5, 10, 15 or 20 mg/kg body weight), or vehicle (PBS) for 21 consecutive days. A caliper was used to monitor the length and width of the tumor every 5 days. The tumor volume (V) was calculated using the following formula: V=(a x b²)/2, where a and b are the maximum and minimum diameters in millimeters, respectively. On the 30th day after cell injection,

the tumor burden was <10% of the body weight and the longest diameter of a single tumor was 12 mm, in line with animal ethics requirements. There were no ulcerated, necrotic or infected tumors. The mice were euthanized with an intraperitoneal injection of pentobarbital sodium (200 mg/kg), and the xenograft tumors were excised and measured.

Quantitative determination of oxidative stress and hematoxylin-eosin staining. Xenograft tumors and livers were collected after the mice were sacrificed under anesthesia. Samples were subsequently fixed with 4% paraformaldehyde in PBS for 24 h at room temperature, dehydrated with an ethanol gradient, cleared with xylene, embedded in paraffin and then cut into 4- μ m sections. Dihydroethidium (DHE; Thermo Fisher Scientific, Inc.) staining was used to determine ROS levels in the xenograft tumors. HepG2 cells and tissue sections were stained with 5 mmol/l DHE (in PBS) for 20 min at room temperature. Nuclei were stained with DAPI at 25°C for 5 min. For H&E staining, the sections were dewaxed and dehydrated, subsequently washed with PBS, and then stained with H&E at 25°C for 2 min each. Observed under a light microscope (X171; Olympus Corporation), in three random sections of each sample, three different areas (or more) were randomly selected for the capture of images at x40 magnification. Analyses were performed using ImageJ 1.8.0 software (National Institutes of Health). Results are shown as the mean \pm SD (n=6 mice per group).

Germacrone-interaction proteins comprehensive analysis. The protein network with germacrone was built using the STITCH tool (<https://stitch.embl.de/>), which includes direct physical interactions between germacrone and the interacting proteins, as well as the inner functional correlation between these proteins. After importing germacrone into the Search Tool STITCH, the germacrone-interaction protein network information was obtained.

Statistical analysis. Each experiment was repeated independently at least three times. The animals were randomly divided into five experimental groups. Survival analysis was performed using the log-rank test. Body weight analysis was performed using repeated measures ANOVA. Unpaired Student's t-test was used to compare two groups. Statistical comparisons between three or more groups were performed using one-way ANOVA followed by Tukey's multiple comparison test. $P < 0.05$ was used to indicate a statistically significant difference. All analyses were performed using GraphPad Prism 7 (GraphPad Software, Inc.).

Results

Effects of GM on HepG2 cell proliferation. The chemical structure of GM is shown in Fig. 1A. To determine whether GM inhibited HepG2 cell viability, cells were treated with different concentrations of GM (0, 50, 100, 150 and 200 μ M) for 12, 24 or 48 h and cell viability was detected using the CCK-8 assay. GM markedly hampered the viability of HepG2 cells in a dose-dependent manner (Fig. 1B), and treatment with 200 μ M of GM for 24 h had the most obvious effect (Fig. 1B). Furthermore, the effect of GM on proliferation was investigated

by treating HepG2 cells with different GM concentrations for 24 h, and then performing the colony-formation assay and EdU staining. These two methods demonstrated that cell proliferation was substantially inhibited by GM treatment, compared with the cell proliferation rate in the control group (Fig. 1C and D). Thereafter, cellular damage or death was evaluated using a 7-AAD cell viability assay kit and flow cytometry. The results revealed that GM increased the damage or death in HepG2 cells in a dose-dependent manner (Fig. 1E).

GM induces plasma membrane permeabilization and pyroptosis in HepG2 cells. Microscopic study of the cells revealed membranous blebbing and the presence of large bubbles emerging from the plasma membrane in GM-treated HepG2 cells, which were distinct from the morphological features of apoptotic cells, but similar to the features of pyroptotic cell morphology (Fig. 2A). To further understand whether these cells underwent pyroptosis in response to GM, the concentration of cytosolic compounds that are released as a result of membrane disruption during pyroptosis, such as LDH, was measured. GM treatment markedly increased the release of LDH into the supernatant in a dose-dependent manner (Fig. 2B). Staining with PI showed that treatment with GM increased PI fluorescence in a dose-dependent manner (Fig. 2C), further indicating the breakdown of plasma membrane integrity. Furthermore, GM treatment substantially increased the cell population positive for Annexin V and PI in a dose-dependent manner, as detected using flow cytometry (Fig. 2D). Altogether, these data indicated that GM induced pyroptotic cell death by plasma membrane permeabilization in HepG2 cells.

According to previous studies, caspases-1/4/5/11 can cleave GSDMD, releasing its N-terminal domain from the membrane and permitting pore formation by GSDMD, thereby inducing pyroptosis (22). Although caspase-1 and GSDMD are expressed in HepG2 cells (31), in the present study, GM treatment did not induce the cleavage of GSDMD and caspase-1, as detected by western blot analysis (Fig. 2E and F). This implied that GSDMD is not involved in GM-induced HepG2 cell death. The discovery and characterization of GSDME are relatively recent and it has been proposed to act as a molecular switch between apoptotic and pyroptotic cell death. When caspase-3 cleaves the N-terminal fragment of GSDME (GSDME-N), apoptotic cell death is converted into pyroptotic cell death (26). Therefore, whether the effector of cell pyrolysis, GSDME (32), is involved in GM-induced cell death was evaluated in the present study. Treatment with GM (150/200 μ M) increased the cleavage of caspase-3, with concomitant increase in the expression levels of GSDME-N (Fig. 2G and H). These data indicated that GM induced the caspase-3-mediated cleavage of GSDME, which is involved in pyroptosis in HepG2 cells.

Caspase-3-mediated cleavage of GSDME involves GM-induced pyroptosis in HepG2 cells. We hypothesized that the activation of caspase-3 is essential for GM-induced pyroptosis. To validate this hypothesis, stable caspase-3-knockdown HepG2 cells were generated and validated by analyzing the expression levels of caspase-3 using RT-qPCR and western blotting (Fig. 3A and B). Knockdown of caspase-3 rescued cell viability in response to GM treatment but resulted in a prominent reduction in GM-induced LDH release and plasma

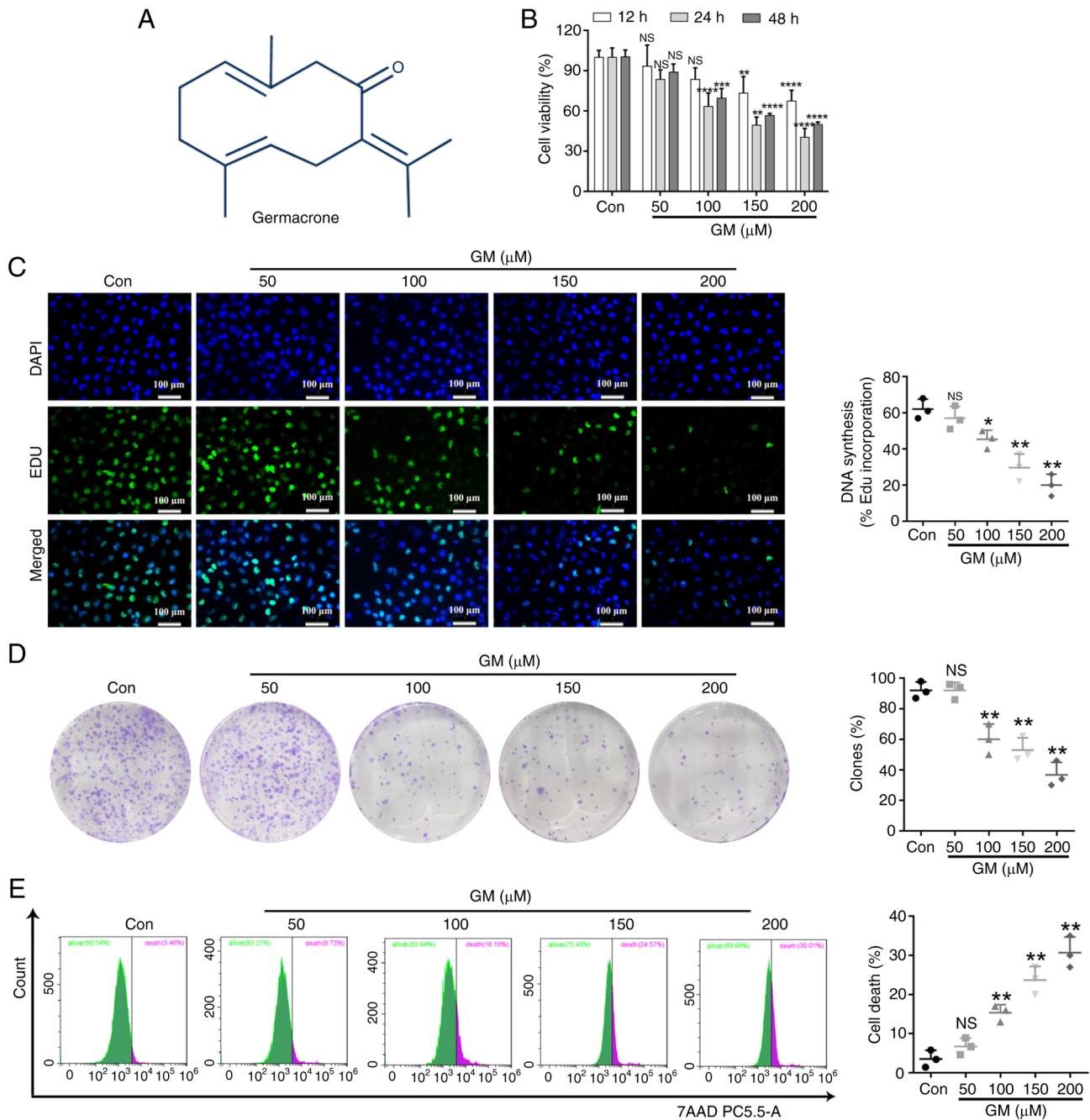


Figure 1. Effects of GM on HepG2 cell growth. (A) Chemical structure of GM. (B) HepG2 cells were treated with the indicated concentrations of GM for 12, 24 or 48 h, and cell viability was evaluated using a Cell Counting Kit-8 assay. HepG2 cells were treated with the indicated concentrations of GM for 24 h, and cell proliferation was evaluated using the (C) BeyoClick™ Edu Cell Proliferation Kit and (D) colony-formation assays. (E) Cell death was assessed using the 7-AAD cell viability assay kit. Results are presented as the mean \pm SD of three independent experiments. * P <0.05, ** P <0.01, *** P <0.001 and **** P <0.0001 vs. control. Scale bar, 50 μ m. GM, germacrone; NS, not significant; Con, control.

membrane ballooning (Fig. 3C-E). PI staining showed that caspase-3 knockdown decreased the rate of cell death, as indicated by PI fluorescence (Fig. 3F). Meanwhile, HepG2 cells treated with GM proceeded rapidly to the Annexin V and PI double-positive stage, while caspase-3 knockdown delayed the process by decreasing the percentage of double-positive cells (Fig. 3G). Finally, western blot analyses showed that the expression level of GSDME-N was notably reduced in GM-treated HepG2 cells in which caspase-3 knockdown was performed compared with that in GM-treated cells without caspase-3 knockdown (Fig. 3H and I). These results showed

that GM activated caspase-3, which in turn cleaved GSDME to induce pyroptosis.

GM induces mitochondrial damage and enhances ROS production in HepG2 cells. In order to elucidate the underlying mechanism by which GM induces caspase-3/GSDME-mediated pyroptosis, the targets of GM were predicted using the STITCH database. The results showed that GM mainly acts on the cytochrome P450 (CYP) system of the mitochondria (Fig. 4A). Since previous studies have shown that mitochondrial damage is closely linked to GSDME-mediated pyroptosis (33-36), the

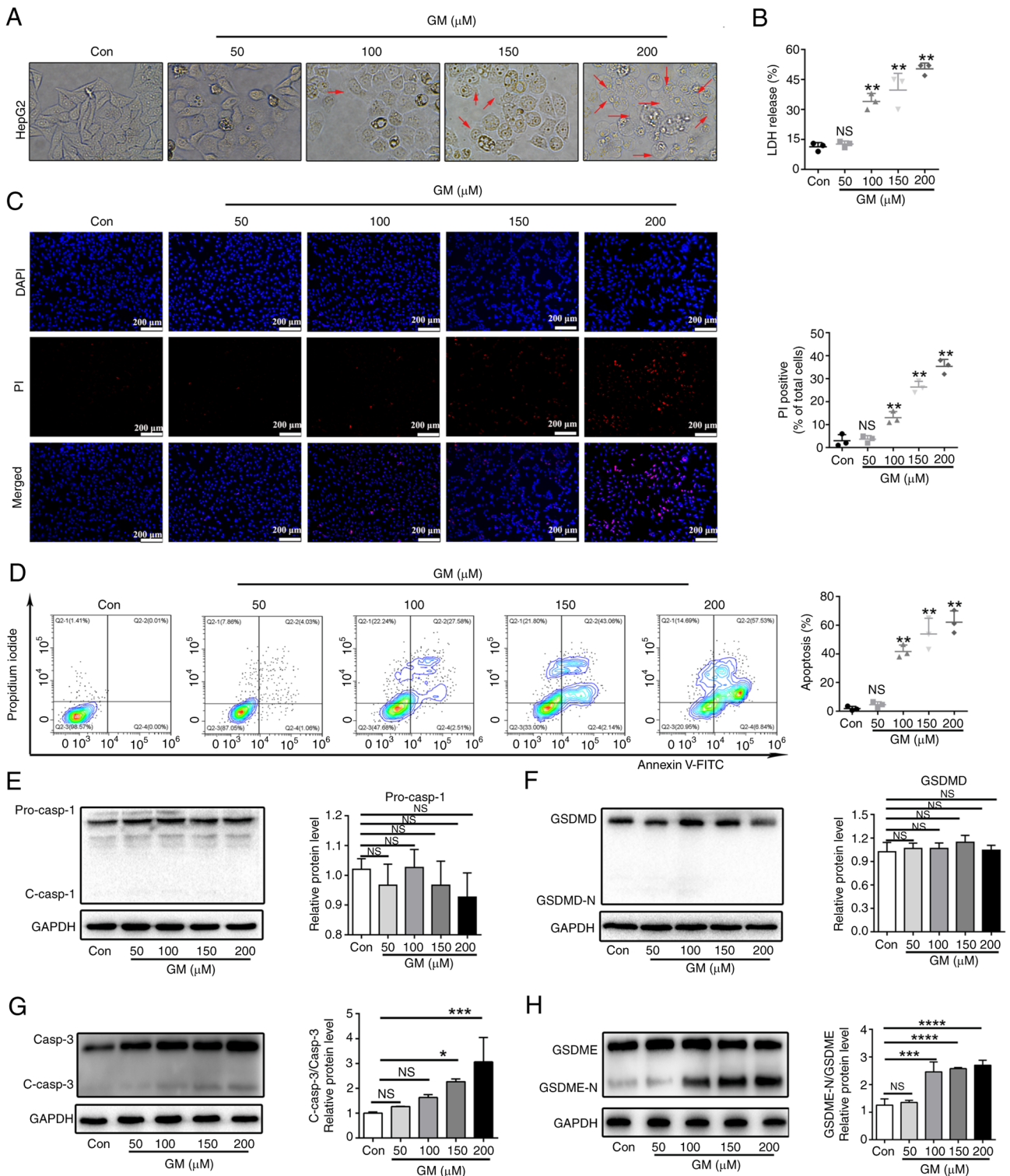


Figure 2. GM induces plasma membrane permeabilization and pyroptosis in HepG2 cells. (A) Representative microscopic images of HepG2 cells treated with GM at different concentrations for 24 h (magnification, $\times 400$). (B) Release of LDH from HepG2 cells treated with GM at different concentrations for 24 h. (C) Fluorescence microscopy images showing PI staining in HepG2 cells. Scale bar, $200 \mu\text{m}$. (D) Representative flow cytometry scatter plots. HepG2 cells were treated with GM at different concentrations for 24 h and then analyzed using flow cytometry. Representative immunoblot analysis of (E) pro-caspase-1 and cleaved caspase-1, (F) GSDMD and GSDMD-N, (G) caspase-3 and cleaved caspase-3 (H) GSDME and GSDME-N, and GAPDH protein expression levels were detected using western blotting analysis in HepG2 cells treated with GM at different concentrations for 24 h. Results are presented as the mean \pm SD of three independent experiments. * $P < 0.05$, ** $P < 0.01$, *** $P < 0.001$ and **** $P < 0.0001$ vs. control. Pro-casp, pro-caspase; GSDMD, gasdermin D; GSDMD-N, gasdermin D-N-terminal; C-casp, cleaved caspase; LDH, lactate dehydrogenase; PI, propidium iodide; Con, control; NS, not significant.

present study investigated whether GM-induced pyroptosis was associated with mitochondrial damage. TEM images showed that the cells treated with GM exhibited markedly

increased mitochondrial swelling compared with the control cells (Fig. 4B). Considering that mitochondrial damage is closely associated with the generation of ROS, we hypothesized

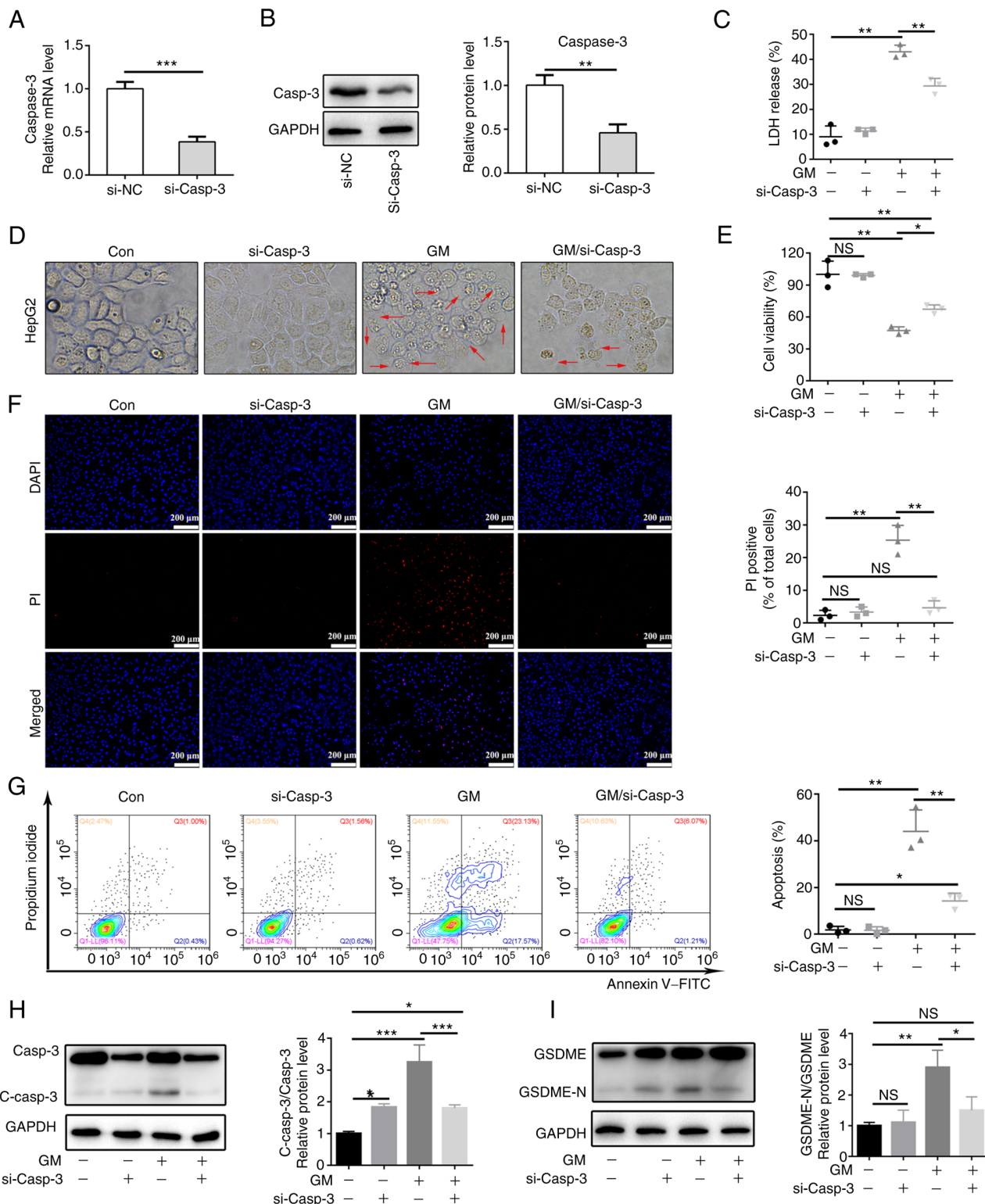


Figure 3. Caspase-3-mediated cleavage of GSDME is involved in GM-induced pyroptosis in HepG2 cells. Expression levels of caspase-3 in si-NC and si-Casp3 cells were detected using (A) reverse transcription-quantitative PCR and (B) western blotting. HepG2 cells and caspase-3-knockdown HepG2 cells were treated with 200 μM GM for 24 h and (C) LDH release was measured, as well as (D) cell morphology (magnification, x400) and (E) cell viability using a Cell Counting kit-8 assay. (F) Fluorescent microscopy images showing PI staining. Scale bar, 200 μm. (G) Representative flow cytometry scatter plots. Representative immunoblot analysis for (H) Casp3 and C-casp3 and (I) GSDME and GSDME-N. Results are represented as the mean ± SD of three independent experiments. *P<0.05, **P<0.01 and ***P<0.001. si-NC, small interfering RNA negative control; Casp3, caspase-3; C-casp3, cleaved caspase-3; GSDME, gasdermin E; GSDME-N, gasdermin E-N-terminal; LDH, lactate dehydrogenase; PI, propidium iodide; GM, germacrone; NS, not significant; Con, control.

that GM increases the levels of cellular ROS. DHE staining revealed that cellular ROS was markedly increased upon treatment with GM in a dose-dependent manner (Fig. 4C).

GM promotes pyroptosis through the induction of ROS in HepG2 cells. It has been reported that caspase-3/GSDME-mediated pyroptosis is closely associated

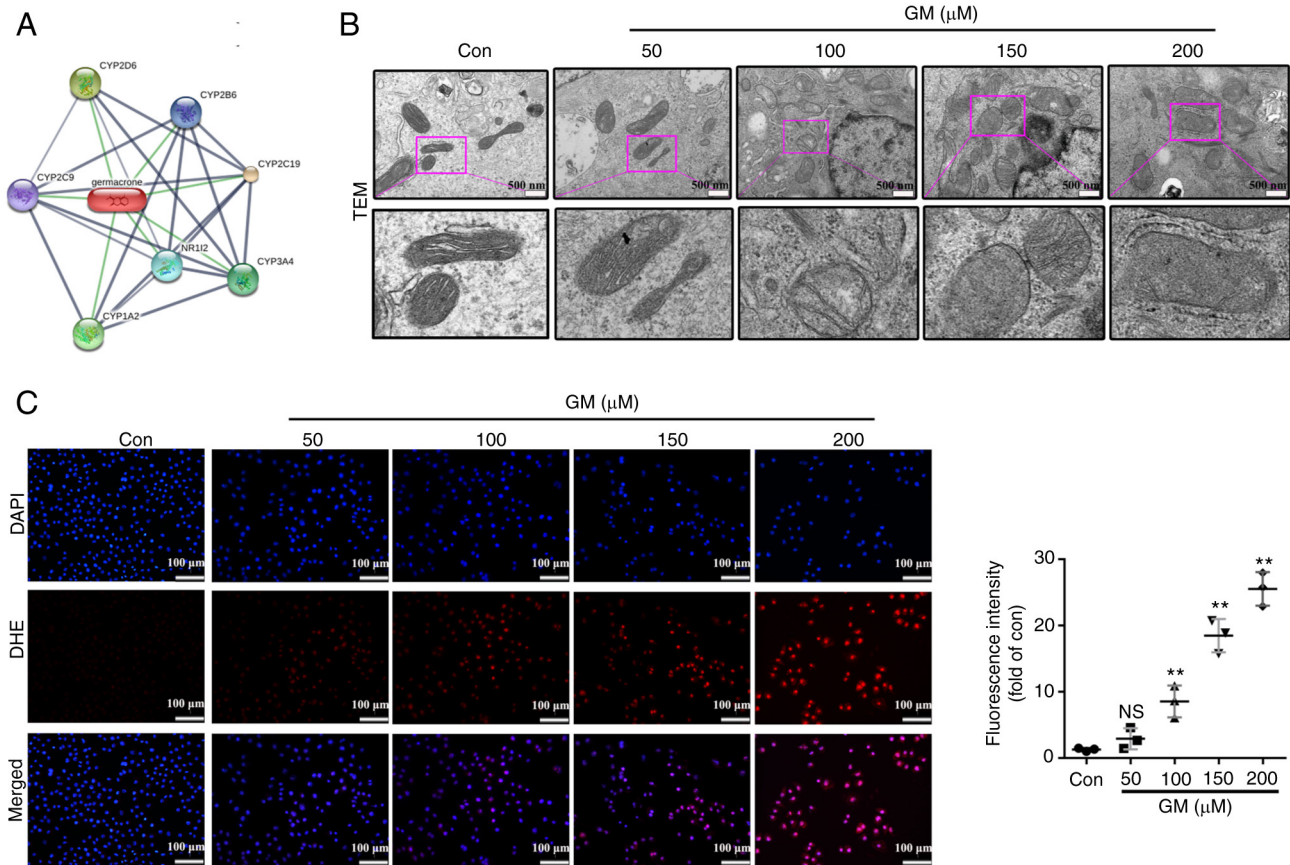


Figure 4. GM induces mitochondrial damage and increases the production of ROS in HepG2 cells. (A) Representative transmission electron microscopy images of HepG2 cells treated with the indicated concentrations of GM for 24 h. Scale bar, 500 nm. (B) Protein-protein interactions between GM-interactors are shown in gray, whereas interactions between GM and its targets are shown in green. Stronger associations are represented by thicker lines. (C) HepG2 cells were treated with the indicated concentrations of GM for 24 h, and cellular ROS levels were detected using DHE (red) and DAPI (blue) staining. Scale bar, 100 μm. Results are represented as the mean ± SD of three independent experiments. ** $P < 0.01$ vs. control. ROS, reactive oxygen species; NS, not significant; Con, control; DHE, dihydroethidium; GM, germacrone; TEM, transmission electron microscopy.

with an increase in ROS production (32). The present study suggested that GM treatment results in an elevation of cellular ROS levels, thereby regulating HepG2 cell pyroptosis. To verify this hypothesis, HepG2 cells were pretreated with the ROS scavenger NAC (5 mM) for 2 h and then treated with GM for 24 h. Notably, NAC substantially attenuated the pyroptotic characteristics, including balloon-like bubbling, the release of LDH, PI staining, pyroptosis, and double positivity for Annexin V and PI (Fig. 5A-E). Additionally, NAC substantially attenuated the cleavage of caspase-3 and GSDME in GM-treated HepG2 cells (Fig. 5F and G). These results implied that GM, by damaging the mitochondria, increased the generation of cellular ROS, and induced pyroptosis by activating caspase-3 and GSDME in HepG2 cells.

GM inhibits tumor growth and induces pyroptosis in a xenograft model. The aforementioned *in vitro* experiments demonstrated that GM-induced pyroptosis via cleaved caspase-3 to exert antitumor effects. To investigate the antitumor effects of GM *in vivo*, HepG2 cells were injected subcutaneously into the right side of BALB/C nude mice and the xenograft tumor volume was measured every 5 days. At 6 days post-cell injection, the nude mice were treated intragastrically with GM solution (5, 10, 15 or 20 mg/kg body weight) or vehicle for 21 consecutive days. The body weight of the mice

did not differ between the GM- and the vehicle-treated groups (Fig. 6A). However, administration of GM markedly attenuated the volume and the weight of the tumors in a dose-dependent manner compared with the corresponding parameters in the vehicle group (Fig. 6B-D). Moreover, higher levels of ROS, determined by stronger fluorescence staining with DHE, were also observed in the GM treatment groups (Fig. 6E). In addition, GM administration substantially promoted the formation of cleaved caspase-3 and GSDME-N in a dose-dependent manner (Fig. 6F and G), which was consistent with the results of the *in vitro* studies on HepG2 cells. Therefore, these results indicated that GM treatment could reduce tumor volume by inducing pyroptosis in a mouse xenograft model. In addition, no significant morphological changes were observed in the liver tissues of the GM-treated mice, suggesting that GM had no significant toxicity in the mice (Fig. 6H).

Discussion

Pyroptosis, a type of programmed cell death, is not cell-type specific and possesses a possible beneficial role in tumor cell therapy. Previous studies have confirmed that bacteria or lipopolysaccharides induce pyroptosis through GSDMD cleavage (37,38). Recent studies have demonstrated that treatment with several chemotherapeutic drugs activates

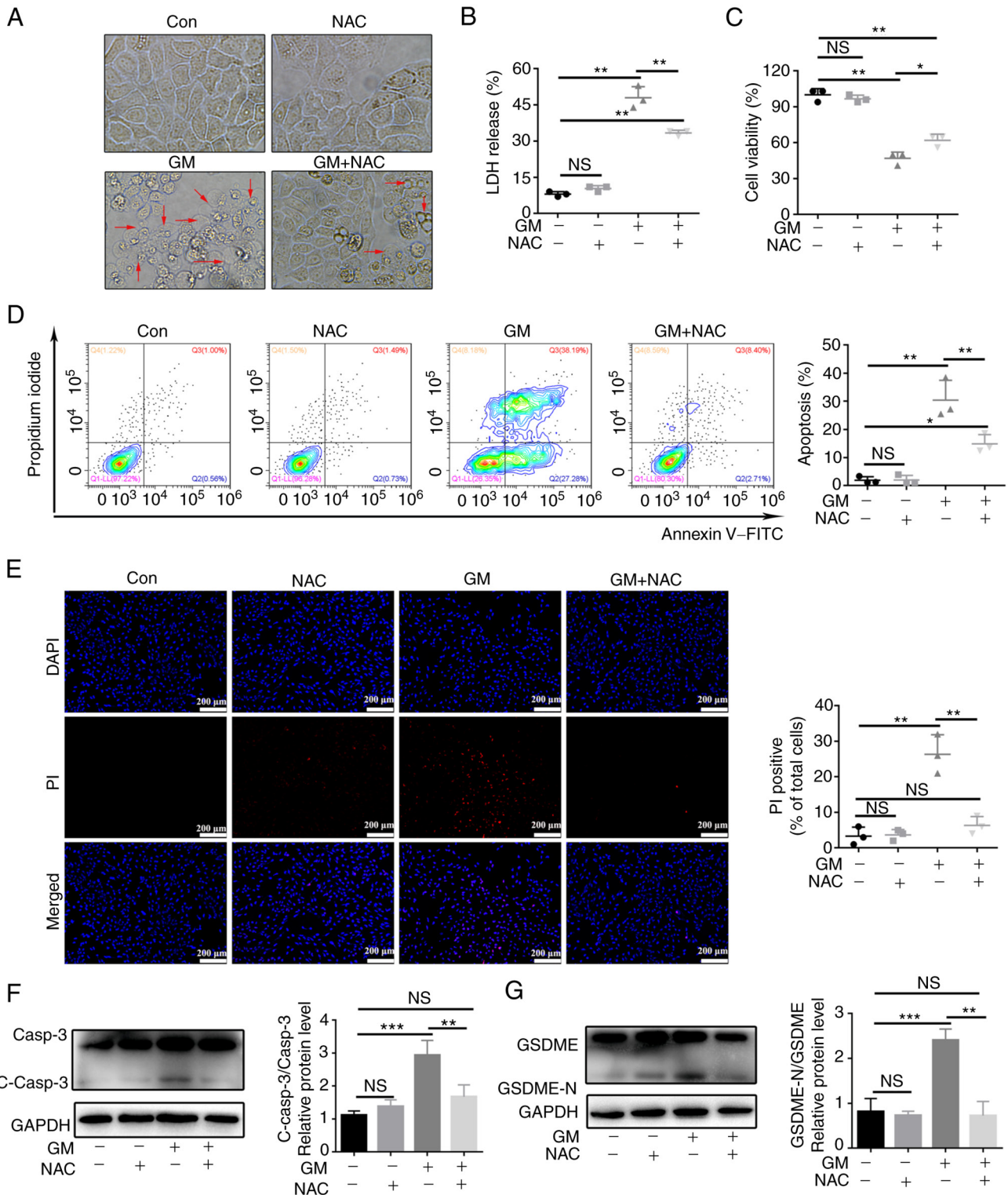


Figure 5. GM promotes pyroptosis through induction of reactive oxygen species in HepG2 cells. HepG2 cells were pretreated with or without 5 mM NAC for 2 h before treatment with 200 μ M of GM for 24 h, following which different assays were performed. (A) HepG2 cell morphology (magnification, x400). (B) Results of the LDH assay. (C) Analysis of cell viability using a Cell Counting kit-8 assay. (D) Representative flow cytometry scatter plots. (E) Fluorescence microscopy images showing PI staining. Scale bar, 200 μ m. (F and G) Representative immunoblot analysis for (F) Casp3 and C-casp3, and (G) GSDME and GSDME-N. Results are presented as mean \pm SD of three independent experiments. *P<0.05, **P<0.01 and ***P<0.001. Casp3, caspase-3; C-casp3, cleaved-caspase-3; GSDME, gasdermin E; GSDME-N, gasdermin E-N-terminal; NAC, N-acetylcysteine; LDH, lactate dehydrogenase; PI, propidium iodide; NS, not significant; Con, control; GM, germacrone.

caspase-3/GSDME and triggers secondary necrosis after apoptosis or pyroptosis (26,39), which challenges a long-standing view that chemotherapy acts most potently by stimulating

apoptosis. Previous studies have shown that GM exerts anticancer effects through multiple molecular mechanisms. For example, GM treatment effectively induces apoptosis by

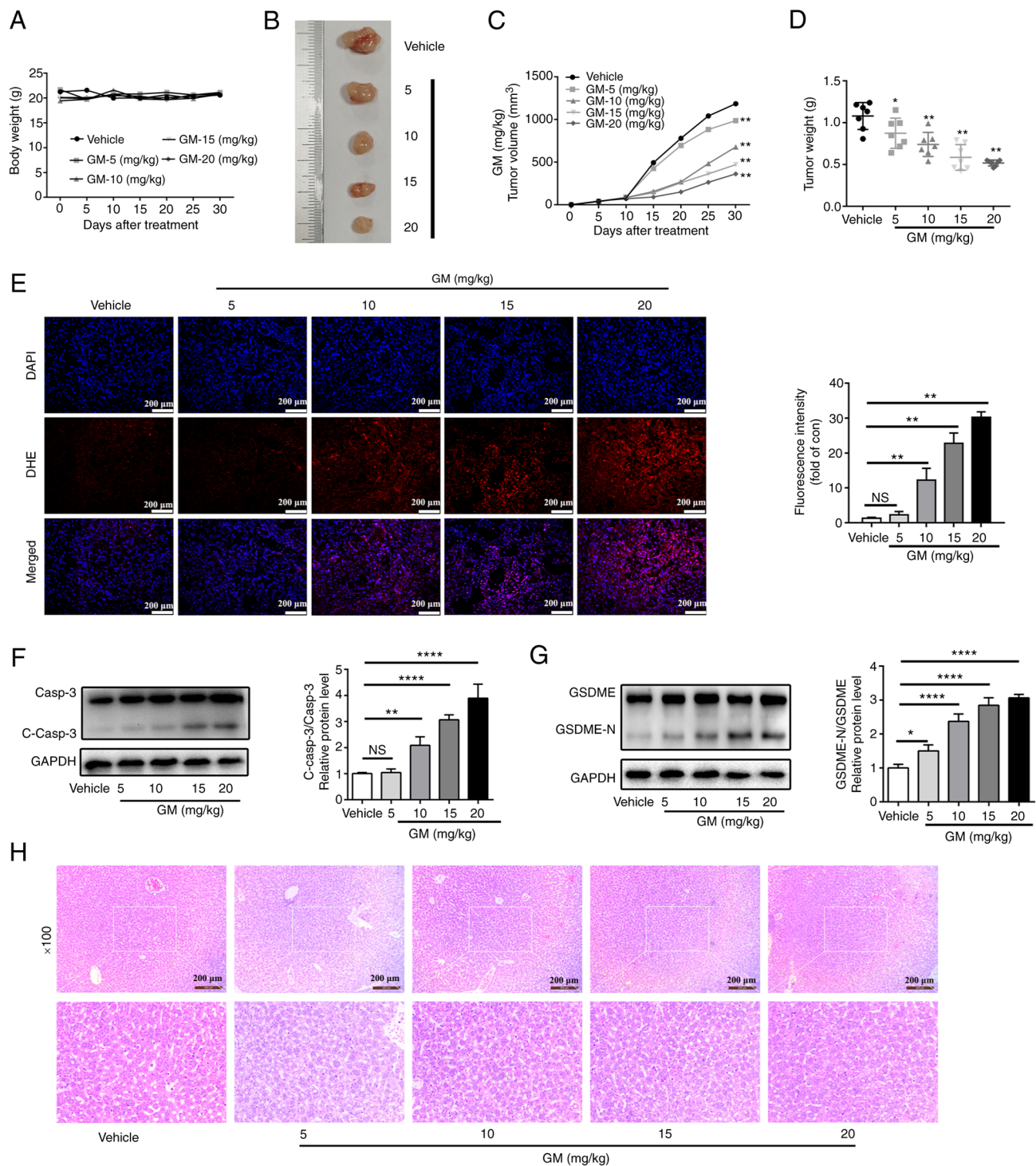


Figure 6. GM inhibits tumor growth and induces pyroptosis in a xenograft model. A total of 1×10^6 HepG2 cells were inoculated into BALB/c nude mice to establish a tumor model. Starting six days after cell injection, the nude mice were treated intragastrically with germacrone solution (0, 5, 10, 15 or 20 mg/kg body weight) for 21 consecutive days. (A) Body weight of mice at 30 days ($n=6$). (B) Representative images of HepG2 cell-derived xenograft tumors on day 30. (C) Tumor volume was measured every 5 days. (D) Tumor weight on day 30. (E) Fluorescence images of DHE (red) and DAPI (blue) staining showing reactive oxygen species levels in tumor sections ($n=3$). Scale bar, 100 μm . (F and G) Western blot images of protein expression of (F) Casp3 and C-casp3, and (G) GSDME and GSDME-N in tumors derived from treatment with GM or vehicle. (H) Representative liver HE staining images of all experimental groups at day 30. Results are presented as mean \pm SD of three independent experiments. * $P<0.05$, ** $P<0.01$ and **** $P<0.0001$, vs. vehicle. Casp3, caspase-3; C-casp3, cleaved-caspase-3; GSDME, gasdermin E; GSDME-N, gasdermin E-N-terminal; NS, not significant; DHE, dihydroethidium; GM, germacrone.

inducing cell cycle arrest in human esophageal squamous cell carcinoma cells, breast cancer cell lines and A549 cells (40,41). Furthermore, other studies have shown that GM induces apoptosis of gastric cancer cells via the regulation of the hepatitis B virus X-interacting protein-mediated cell cycle and

promoting the formation of autophagosomes, (42) and induces apoptosis in HepG2 cells by downregulating the activation of the JAK2/STAT3 pathway and upregulating the expression of p53 and Bax (43). However, whether pyroptosis is involved in the chemotherapeutic use of GM in HepG2 cells still remains

unclear. The present study demonstrated that GM induced pyroptosis of HepG2 cells via a ROS-caspase3-GSDME pathway. In HepG2 cells, GM caused mitochondrial damage and elevated ROS, consequently activating caspase-3, and initiated the cleavage of GSDME, ultimately inducing pyroptosis of HepG2 cells. These findings shed light on the interassociation between GM and pyroptosis, and suggested a functional role for GM-mediated pyroptosis in antitumor treatment.

Consistent with previous results, cell viability and proliferation assays demonstrated that GM effectively inhibited the proliferation of HepG2 cells in a concentration-dependent manner. Moreover, a flow cytometry assay revealed that GM treatment induced an increase in the HepG2 cell mortality rate. In addition, it was observed that GM induced LDH release and cell swelling, and these results suggested that other types of cell death, such as pyroptosis and necroptosis, may also be involved in GM-induced HepG2 cell death. Further experiments showed that GSDMD and caspase-1 were not activated by GM in HepG2 cells; however, GSDME activation was observed both *in vivo* and *in vitro*. Furthermore, the *in vivo* and *in vitro* results showed that the level of cleaved-caspase-3 protein was positively associated with the sensitivity of cells to pyroptosis induced by GM exposure. These results indicated that caspase-3 may be crucial for GM-induced pyroptosis. Notably, in caspase-3-depleted HepG2 cells, the LDH release and pyroptosis induced by GM were decreased, indicating that the pyroptosis induced by GM was caspase-3-dependent. Consistently, flow cytometry data showed that caspase-3 knockdown rescued cell death caused by GM and that it reduced the proportion of Annexin V-PI single-positive cells, while it decreased the proportion of double-positive cells. Altogether, these data indicated that GM can induce pyroptosis via the caspase-3/GSDME pathway in HepG2 cells.

Next, the mechanism by which GM regulates caspase-3/GSDME-mediated pyroptosis in HepG2 cells was explored by predicting the protein targets of GM using STITCH. It was found that GM mainly acts on the CYPs of the mitochondria. CYPs are primarily located in the inner membrane of the mitochondria and are the pivotal enzymes involved in the oxidative metabolism of drugs and exogenous substances (44-46). Dysfunctional CYPs can affect the cellular redox balance, resulting in increased cellular ROS production (47-49). Previous studies have shown that ROS play an important role in pyroptosis (26,50). For example, lobaplatin induces caspase-3/GSDME-mediated pyrolysis by increasing cellular ROS levels in colon cancer cells (32). Iron-activated ROS promotes the oxidation of the outer mitochondrial membrane protein Tom20 in melanoma cells and induces pyrolysis by activating the Bax/caspase-3/GSDME pathway (50). Another critical study showed that GM increases ROS production and induces apoptosis in HepG2 cells (43). These reports collectively suggest that besides apoptosis, ROS can induce cell death towards the pyroptosis pathway. Hence, in the present study, we hypothesized that GM might enhance the generation of ROS to promote apoptosis and caspase-3/GSDME-mediated pyroptosis by targeting the mitochondria in HepG2 cells. Notably, TEM showed that GM markedly increased mitochondrial swelling compared with that observed in the control cells, and that it increased ROS levels. However, the addition of the antioxidant NAC markedly blocked

pyroptotic characteristics after GM treatment. Moreover, NAC blocked the release of LDH and cleaved caspase-3/GSDME induced by GM. These results indicated that GM markedly elevated the generation of cellular ROS by damaging mitochondria to induce caspase-3/GSDME-mediated pyroptosis in HepG2 cells.

However, the present study has some limitations. First, further investigations are warranted to confirm the effect of GM on liver cancer cells. Therefore, future studies will include the verification of the inhibitory effect and mechanism of GM in different liver cancer cell lines. Furthermore, the expression of GSDME should have been suppressed to demonstrate that the cell death observed in HepG2 cells was due to GSDME-mediated pyroptosis and not the other types of cell death. Although GM increases the production of ROS by inducing mitochondrial damage, the mechanism of GM-induced mitochondrial damage is not fully elucidated. Future studies should investigate the effect of GM on the regulatory mechanism related to mitochondria in liver cancer cells.

The findings of the present study demonstrated that GM might be a potential candidate for the treatment of liver cancer, and that GM triggered pyroptosis by activating caspase-3/GSDME. These findings provide a novel insight that ROS/caspase-3/GSDME-dependent pyroptosis is a possible mechanism through which GM exerts its therapeutic action.

Acknowledgements

Not applicable.

Funding

The current study was supported by grants from the Shenzhen Science and Technology Project (nos. JCYJ20170817094901026 and JCYJ20180302173542393).

Availability of data and materials

The raw data and original images from the study are included in the Figshare database (<https://doi.org/10.6084/m9.figshare.19233756.v1>). Further inquiries can be directed to the corresponding authors.

Authors' contributions

XZZ and XFS conceived the study concept and revised the manuscript. XFS, XZ and WFM performed the experiments and drafted the original manuscript. WXF, QH, MQM, MLL and RH participated in conducting the study and the data analysis. ZYH and JL analyzed the data, contributed to writing the paper, and revised the paper. XZZ was responsible for the funding acquisition. XFS and XZ confirm the authenticity of all the raw data. All authors read and approved the final manuscript.

Ethics approval and consent to participate

All experiments were approved by and performed in accordance with the relevant guidelines and regulations drafted by the Animal Ethics Committee of Guangzhou University of Chinese Medicine (approval no. 20210303042).

Patient consent for publication

Not applicable.

Competing interests

The authors declare that they have no competing interests.

References

- Clark T, Maximin S, Meier J, Pokharel S and Bhargava P: Hepatocellular carcinoma: Review of epidemiology, screening, imaging diagnosis, response assessment, and treatment. *Curr Probl Diagn Radiol* 44: 479-486, 2015.
- Hartke J, Johnson M and Ghabril M: The diagnosis and treatment of hepatocellular carcinoma. *Semin Diagn Pathol* 34: 153-159, 2017.
- Sia D, Villanueva A, Friedman SL and Llovet JM: Liver cancer cell of origin, molecular class, and effects on patient prognosis. *Gastroenterology* 152: 745-761, 2017.
- Sung H, Ferlay J, Siegel RL, Laversanne M, Soerjomataram I, Jemal A and Bray F: Global cancer statistics 2020: GLOBOCAN estimates of incidence and mortality worldwide for 36 cancers in 185 countries. *CA Cancer J Clin* 71: 209-249, 2021.
- Oravec M and Mészáros J: Traditional Chinese medicine: Theoretical background and its use in China. *Orv Hetil* 153: 723-731, 2012 (In Hungarian).
- Chan HHL and Ng T: Traditional Chinese medicine (TCM) and allergic diseases. *Curr Allergy Asthma Rep* 20: 67, 2020.
- Zhou P: Traditional Chinese medicine. *Comb Chem High Throughput Screen* 13: 836, 2010.
- Momenkiaei F and Raofie F: Preparation of Curcuma longa L. extract nanoparticles using supercritical solution expansion. *J Pharm Sci* 108: 1581-1589, 2019.
- Dosoky NS and Setzer WN: Chemical composition and biological activities of essential oils of *Curcuma* species. *Nutrients* 10: 1196, 2018.
- Sun J, Chen F, Braun C, Zhou YQ, Rittner H, Tian YK, Cai XY and Ye DW: Role of curcumin in the management of pathological pain. *Phytomedicine* 48: 129-140, 2018.
- Ayati Z, Ramezani M, Amiri MS, Moghadam AT, Rahimi H, Abdollahzade A, Sahebkar A and Emami SA: Ethnobotany, phytochemistry and traditional uses of *Curcuma* spp. and pharmacological profile of two important species (*C. longa* and *C. zedoaria*): A review. *Curr Pharm Des* 25: 871-935, 2019.
- Li Y, Wu Y, Li Y and Guo F: Review of the traditional uses, phytochemistry, and pharmacology of *Curcuma wenyujin* Y. H. Chen et C. Ling. *J Ethnopharmacol* 269: 113689, 2021.
- Dosoky NS, Satyal P and Setzer WN: Variations in the volatile compositions of *Curcuma* species. *Foods* 8: 53, 2019.
- Goel A and Aggarwal BB: Curcumin, the golden spice from Indian saffron, is a chemosensitizer and radiosensitizer for tumors and chemoprotector and radioprotector for normal organs. *Nutr Cancer* 62: 919-930, 2010.
- Giordano A and Tommonaro G: Curcumin and cancer. *Nutrients* 11: 2376, 2019.
- Burapan S, Kim M, Paisooksantivatana Y, Eser BE and Han J: Thai *Curcuma* species: Antioxidant and bioactive compounds. *Foods* 9: 1219, 2020.
- Srivilai J, Waranuch N, Tangsumranjit A, Khorana N and Ingkaninan K: Germacrone and sesquiterpene-enriched extracts from *Curcuma aeruginosa* Roxb. Increase skin penetration of minoxidil, a hair growth promoter. *Drug Deliv Transl Res* 8: 140-149, 2018.
- Liu Y, Wang W, Fang B, Ma F, Zheng Q, Deng P, Zhao S, Chen M, Yang G and He G: Anti-tumor effect of germacrone on human hepatoma cell lines through inducing G2/M cell cycle arrest and promoting apoptosis. *Eur J Pharmacol* 698: 95-102, 2013.
- Riaz A, Rasul A, Kanwal N, Hussain G, Shah MA, Sarfraz I, Ishfaq R, Batool R, Rukhsar F and Adem S: Germacrone: A potent secondary metabolite with therapeutic potential in metabolic diseases, cancer and viral infections. *Curr Drug Metab* 21: 1079-1090, 2020.
- Zhang R, Hao J, Guo K, Liu W, Yao F, Wu Q, Liu C, Wang Q and Yang X: Germacrone inhibits cell proliferation and induces apoptosis in human esophageal squamous cell carcinoma cells. *Biomed Res Int* 2020: 7643248, 2020.
- Kovacs SB and Miao EA: Gasdermins: Effectors of pyroptosis. *Trends Cell Biol* 27: 673-684, 2017.
- Shi J, Gao W and Shao F: Pyroptosis: Gasdermin-mediated programmed necrotic cell death. *Trends Biochem Sci* 42: 245-254, 2017.
- Jia C, Chen H, Zhang J, Zhou K, Zhuge Y, Niu C, Qiu J, Rong X, Shi Z, Xiao J, *et al*: Role of pyroptosis in cardiovascular diseases. *Int Immunopharmacol* 67: 311-318, 2019.
- Shi J, Zhao Y, Wang K, Shi X, Wang Y, Huang H, Zhuang Y, Cai T, Wang F and Shao F: Cleavage of GSDMD by inflammatory caspases determines pyroptotic cell death. *Nature* 526: 660-665, 2015.
- Sun L, Ma W, Gao W, Xing Y, Chen L, Xia Z, Zhang Z and Dai Z: Propofol directly induces caspase-1-dependent macrophage pyroptosis through the NLRP3-ASC inflammasome. *Cell Death Dis* 10: 542, 2019.
- Wang Y, Gao W, Shi X, Ding J, Liu W, He H, Wang K and Shao F: Chemotherapy drugs induce pyroptosis through caspase-3 cleavage of a gasdermin. *Nature* 547: 99-103, 2017.
- Jiang M, Qi L, Li L and Li Y: The caspase-3/GSDME signal pathway as a switch between apoptosis and pyroptosis in cancer. *Cell Death Discov* 6: 112, 2020.
- Liang WF, Gong YX, Li HF, Sun FL, Li WL, Chen DQ, Xie DP, Ren CX, Guo XY, Wang ZY, *et al*: Curcumin activates ROS signaling to promote pyroptosis in hepatocellular carcinoma HepG2 cells. *In Vivo* 35: 249-257, 2021.
- Zhang X, Zhang P, An L, Sun N, Peng L, Tang W, Ma D and Chen J: Miltirone induces cell death in hepatocellular carcinoma cell through GSDME-dependent pyroptosis. *Acta Pharm Sin B* 10: 1397-1413, 2020.
- Livak KJ and Schmittgen TD: Analysis of relative gene expression data using real-time quantitative PCR and the 2(-Delta Delta C(T)) method. *Methods* 25: 402-408, 2001.
- Zhan ZY, Wu M, Shang Y, Jiang M, Liu J, Qiao CY, Ye H, Lin YC, Piao MH, Sun RH, *et al*: Taxifolin ameliorate high-fat-diet feeding plus acute ethanol binge-induced steatohepatitis through inhibiting inflammatory caspase-1-dependent pyroptosis. *Food Funct* 12: 362-372, 2021.
- Yu J, Li S, Qi J, Chen Z, Wu Y, Guo J, Wang K, Sun X and Zheng J: Cleavage of GSDME by caspase-3 determines lobaplatin-induced pyroptosis in colon cancer cells. *Cell Death Dis* 10: 193, 2019.
- Kleih M, Böpple K, Dong M, Gaißler A, Heine S, Olayoye MA, Aulitzky WE and Essmann F: Direct impact of cisplatin on mitochondria induces ROS production that dictates cell fate of ovarian cancer cells. *Cell Death Dis* 10: 851, 2019.
- Li Q, Liang X, Yang Y, Zeng X, Zhong X and Huang C: Panax notoginseng saponins ameliorate cisplatin-induced mitochondrial injury via the HIF-1 α /mitochondria/ROS pathway. *FEBS Open Bio* 10: 118-126, 2020.
- Mazat JP, Devin A and Ransac S: Modelling mitochondrial ROS production by the respiratory chain. *Cell Mol Life Sci* 77: 455-465, 2020.
- Li Q, Shi N, Cai C, Zhang M, He J, Tan Y and Fu W: The role of mitochondria in pyroptosis. *Front Cell Dev Biol* 8: 630771, 2021.
- Wang K, Sun Q, Zhong X, Zeng M, Zeng H, Shi X, Li Z, Wang Y, Zhao Q, Shao F and Ding J: Structural mechanism for GSDMD targeting by autoprocessed caspases in pyroptosis. *Cell* 180: 941-955.e20, 2020.
- Wu LS, Liu Y, Wang XW, Xu B, Lin YL, Song Y, Dong Y, Liu JL, Wang XJ, Liu S, *et al*: LPS enhances the chemosensitivity of oxaliplatin in HT29 cells via GSDMD-mediated pyroptosis. *Cancer Manag Res* 12: 10397-10409, 2020.
- An H, Heo JS, Kim P, Lian Z, Lee S, Park J, Hong E, Pang K, Park Y, Oshima A, *et al*: Tetraarsenic hexoxide enhances generation of mitochondrial ROS to promote pyroptosis by inducing the activation of caspase-3/GSDME in triple-negative breast cancer cells. *Cell Death Dis* 12: 159, 2021.
- Zhao Y, Cai J, Shi K, Li H, Du J, Hu D, Liu Z and Wang W: Germacrone induces lung cancer cell apoptosis and cell cycle arrest via the Akt/MDM2/p53 signaling pathway. *Mol Med Rep* 23: 452, 2021.
- Zhong Z, Chen X, Tan W, Xu Z, Zhou K, Wu T, Cui L and Wang Y: Germacrone inhibits the proliferation of breast cancer cell lines by inducing cell cycle arrest and promoting apoptosis. *Eur J Pharmacol* 667: 50-55, 2011.
- Fang X, Tan T, Gao B, Zhao Y, Liu T and Xia Q: Germacrone regulates HBXIP-mediated cell cycle, apoptosis and promotes the formation of autophagosomes to inhibit the proliferation of gastric cancer cells. *Front Oncol* 10: 537322, 2020.

43. Liu YY, Zheng Q, Fang B, Wang W, Ma FY, Roshan S, Banafa A, Chen MJ, Chang JL, Deng XM, *et al*: Germacrone induces apoptosis in human hepatoma HepG2 cells through inhibition of the JAK2/STAT3 signalling pathway. *J Huazhong Univ Sci Technolog Med Sci* 33: 339-345, 2013.
44. Cui Y, Peng Y, Zhang Q, Xia S, Ruan B, Xu Q, Yu X, Zhou T, Liu H, Zeng D, *et al*: Disruption of EARLY LESION LEAF 1, encoding a cytochrome P450 monooxygenase, induces ROS accumulation and cell death in rice. *Plant J* 105: 942-956, 2021.
45. He L, He T, Farrar S, Ji L, Liu T and Ma X: Antioxidants maintain cellular redox homeostasis by elimination of reactive oxygen species. *Cell Physiol Biochem* 44: 532-553, 2017.
46. Lu Y and Cederbaum AI: Cytochrome P450s and alcoholic liver disease. *Curr Pharm Des* 24: 1502-1517, 2018.
47. Chien Y, Rosal K and Chung BC: Function of CYP11A1 in the mitochondria. *Mol Cell Endocrinol* 441: 55-61, 2017.
48. Peter Guengerich F and Avadhani NG: Roles of cytochrome P450 in metabolism of ethanol and carcinogens. *Adv Exp Med Biol* 1032: 15-35, 2018.
49. Guengerich FP: Cytochrome P450 2E1 and its roles in disease. *Chem Biol Interact* 322: 109056, 2020.
50. Zhou B, Zhang JY, Liu XS, Chen HZ, Ai YL, Cheng K, Sun RY, Zhou D, Han J and Wu Q: Tom20 senses iron-activated ROS signaling to promote melanoma cell pyroptosis. *Cell Res* 28: 1171-1185, 2018.



This work is licensed under a Creative Commons Attribution-NonCommercial-NoDerivatives 4.0 International (CC BY-NC-ND 4.0) License.